Navier-Stokes Analysis of Muzzle-Blast-Type Waves

O. Baysal*
Old Dominion University, Norfolk, Virginia

A Navier-Stokes solution is presented as a mathematical model to muzzle-blast-type waves. The study has two novel features. First, it is a combined internal/external analysis relating barrel flow parameters to muzzle environment parameters. Second, the dissipative and dispersive effects of viscosity on the propagation phenomenon are captured. The investigation also serves as a numerical analysis of axisymmetric, high-pressure waves in an unsteady, viscous flow. Conservation-form Navier-Stokes equations are integrated by a two-step, explicit finite-difference scheme. The shocks are captured and treated by the inclusion of artificial dissipative terms. Turbulence is accounted for by an algebraic eddy-viscosity model. The internal flow is solved by a predictor-corrector method of characteristics with the shock fitted in; its results compare very well with the experimental data available. The numerical results obtained simulate the muzzle blast waves and show the effects of viscosity. Comparison with the classical spherical blast wave theory shows the deviation in propagation patterns of the axisymmetric and spherical waves.

Nomenclature

a	= local speed of sound, m/s
c_p	= specific heat at constant pressure, J/kg-K
D	= diameter, m
E	= energy per unit volume, J/m^3
k	= thermal conductivity, W/m-K
ℓ	= mixing length, m
M	= momentum vector, kg/m^{2}s
m	= radial momentum, kg/m^{2}s
n	= axial momentum, kg/m^{2}s
p	= pressure, N/m^2
PAMB	= ambient pressure, N/m^2
Pr	= Prandtl number
q	= heat, W/m^2
r	= radial coordinate, m
t	= time, s
u,v	= axial and radial velocity components, respectively, m/s
ZBRRL	= barrel length, m
z	= axial coordinate, m
$\Delta r, \Delta z$	= spatial steps in radial and axial directions, respectively, m
Δt	= time step, s
μ,λ	= first and second coefficients of viscosity, N-s/m^2
ρ	= density, kg/m^3
τ	= shear stress, N/m^2
ω	= vorticity, 1/s

Subscripts and Superscripts

m	= molecular value
N	= index for time
r,z	= index for radial and axial directions, respectively
t	= turbulent value
w	= wall value
0	= reference value
$(\bar{\ })$	= predicted value

Received March 22, 1985; revision received Sept. 11, 1985.

*Assistant Professor, Department of Mechanical Engineering and Mechanics. Member AIAA.

Introduction

THE propagation of muzzle blast waves has received considerable attention due to its direct impact on the design of the tube launchers of projectiles, conventional powder guns, gas guns, and light-gas guns. These pressure waves have large-amplitude, steep or nonsteep fronts that propagate at significantly high speeds. A thorough comprehension of the muzzle blast plays an important role in the achievement of improved muzzle performance, i.e., a higher projectile velocity with a lower blast overpressure. The experimentally observed structure of the muzzle blast[1,2] is an impulsively generated, underexpanded, anisotropic jet that shrinks and collapses toward the muzzle. An acoustic-optical phenomenon (flash) occurs behind the blast shock. At present, the interaction of flash with the muzzle flow bearing the high-pressure waves is not well described. The temperature rise from the flow deceleration through the shocks enhances this phenomenon.

The principles of the classical blast wave theory[3-5] have restrictions relative to its applicability due to the requirement of a spherically symmetric flowfield and a power-law rate of energy dissipation. Because the muzzle blast and the expansion of related flows are highly time-dependent, the quasi-steady-state theory can predict only the instantaneous jet structures. Therefore, this theory is inadequate. The mathematical statement of a model that describes the varieties of fluid-mechanical and energy-transfer phenomena included in the muzzle blast is a set of partial differential equations which does not have a closed-form solution. Various numerical solutions have been reported in the past decade[6-11] for different muzzle-blast cases. All of them are Eulerian solutions, therefore, they do not include the effects of viscosity. Some[8] of the cases assume spherical symmetry and none of them relate the blast flow parameters to the internal flow parameters. Yet the propagation and decay of the high-pressure waves of muzzle blast are strong functions of the internal flow histories and the dissipative effects of viscosity. This investigation emphasizes these effects through a Navier-Stokes solution with the philosophy of simulating the physics of the high-pressure waves as realistic as possible, yet keeping the numerics as simple as possible.[12,13] It is intended to enhance the qualitative and quantitative analysis, and guide the future comprehensive simulations of this complicated phenomenon. As all other numerical studies, this is a valuable means to reduce the matrix of experimental studies and guide the design.

Muzzle Environment Flows

The flow in the barrel is induced by the projectile and the rapid expansion of the pressurized propellant gases. It consists of two separate parts interacting through the motion of the projectile. Almost immediately after the projectile starts to move, a moving normal shock is generated. The initial time and location of this shock are calculated[14] and the pressure ratio is obtained by the shock-tube equations. The external flow is initiated with the ejection of this shock (precursor shock) and accentuated with the base of the projectile clearing the muzzle plane to cause the precursor/propellant flow interactions. This high-Reynolds-number flow has strong convection in one predominant direction and secondary flows in the transverse coordinate plane. It is evident from the experimental data[1,2] that, in addition to the precursor and blast shocks, there exist secondary compression pulses in the viscous shear layers of the propellant-free air mixture. The analytical information of these pulses is still not adequate. The propagation velocities of the blast waves are not constant. They are larger near the source and decrease very rapidly as the wave moves away. This is due to the fact that energy dissipation is more significant in high-pressure waves than in small-amplitude waves. Their propagation pattern and mechanism are deviant from those of the spherical waves.[13]

Model Formulation

Mathematical Statement

Due to axial symmetry, calculations need only be carried out at the intersection of the muzzle environment and the vertical plane, which reduces the number of spatial variables from 3 to 2. Also, to avoid the multiphase and mixing-flow considerations, the propellant is assumed to be a gas identical to the ambient air, and there are no chemical reactions inside or outside the barrel. The governing equations, therefore, are the Navier-Stokes equations, written in strong conservation form, and the Nobel-Abel equation of state:

$$\frac{\partial U}{\partial t}+\frac{\partial F}{\partial z}+\frac{1}{r}\frac{\partial}{\partial r}(rG)+\frac{H}{r}=0 \tag{1}$$

and

$$p=\rho RT/(1-\beta\rho) \tag{2}$$

where

$$U=\begin{bmatrix}\rho\\ n\\ m\\ E\end{bmatrix} \qquad F=\begin{bmatrix}n\\ p+\dfrac{n^2}{\rho}-\tau_{zz}\\ \dfrac{mn}{\rho}-\tau_{zr}\\ (E+p-\tau_{zz})\left(\dfrac{n}{\rho}\right)-\tau_{zr}\left(\dfrac{m}{\rho}\right)-q_z\end{bmatrix}$$

$$G=\begin{bmatrix}m\\ \dfrac{mn}{\rho}-\tau_{zr}\\ p+\dfrac{m^2}{\rho}-\tau_{rr}\\ (E+p-\tau_{rr})\left(\dfrac{m}{\rho}\right)-\tau_{zr}\left(\dfrac{n}{\rho}\right)-q_r\end{bmatrix} \qquad H=\begin{bmatrix}0\\ 0\\ -p+R\\ 0\end{bmatrix}$$

and

$$R=\lambda\nabla\cdot\boldsymbol{M}+2\mu\frac{1}{r}\left(\frac{m}{\rho}\right) \tag{3}$$

The constant β in the Nobel-Abel state equation is assigned a value of 0.001 in this study. The axial, radial, and tangential stress terms and heat-transfer terms are as follows:

$$\tau_{zz}=\lambda\nabla\cdot\boldsymbol{M}+2\mu\frac{\partial}{\partial z}\left(\frac{n}{\rho}\right) \tag{4}$$

$$\tau_{rr}=\lambda\nabla\cdot\boldsymbol{M}+2\mu\frac{\partial}{\partial r}\left(\frac{m}{\rho}\right) \tag{5}$$

$$\tau_{zr}=\mu\left[\frac{\partial}{\partial z}\left(\frac{m}{\rho}\right)+\frac{\partial}{\partial r}\left(\frac{n}{\rho}\right)\right] \tag{6}$$

$$q_z=k\frac{\partial T}{\partial z}, \quad q_r=k\frac{\partial T}{\partial r} \tag{7}$$

The first coefficient of viscosity and the thermal conductivity are given as the sum of their molecular and eddy components:

$$\mu=\mu_m+\mu_t \tag{8}$$

and

$$k=c_p\left(\frac{\mu_m}{Pr_m}+\frac{\mu_t}{Pr_t}\right) \tag{9}$$

The molecular viscosity is assumed to obey Sutherland's formula, and the second coefficient of viscosity is assumed to obey Stokes' formula:

$$\mu_m=\mu_{m,0}\left(\frac{T}{T_0}\right)^{3/2}\left(\frac{T_0+b}{T+b}\right) \tag{10}$$

$$\lambda=-(2/3)\mu \tag{11}$$

where b is the Sutherland constant.

Boundary Conditions

The characteristic of these partial differential equations is mixed hyperbolic-parabolic. However, due to the larger relative order of magnitude of the convective terms, the equations may be considered predominantly hyperbolic. Therefore, this is a marching-type problem which requires boundary conditions as well as initial conditions.

The physical bounds in this computational domain are the external surface of the barrel, and the surface of the projectile when it is ejected (Fig. 1). The impermeability and no-slip conditions are imposed at these solid boundaries. Also, the zero pressure gradient is assumed normal to these surfaces. The temperature variation is neglected (isothermal) on the solid surfaces. The outer boundary (transmittive boundary) should be treated not to permit any nonphysical reflections or accumulation of vorticity. In the present model, they are treated by a first-degree interpolation of the property values, i.e., their gradients are prescribed from the domain of computation. The muzzle plane properties are dictated by the internal flow calculations for a supersonic exit flow. In case of subsonic ejection, the external and internal influences are accounted for so as to satisfy the conservation of mass. The axis of symmetry has no mass or energy transfer across it, therefore, the radial momentum vanishes on the centerline. Also, to obtain smooth property profiles across the axis of symmetry, the radial gradients of the properties are set equal to zero on the centerline. The terms with the $(1/r)$ factor in the governing equations are treated using the L'Hospital rule as r approaches zero on the axis of symmetry, i.e.,

$$\lim_{r\to 0}\left[\frac{1}{r}\frac{\partial}{\partial r}(rG)\right]=\lim_{r\to 0}\left[2\frac{\partial G}{\partial r}\right] \tag{12}$$

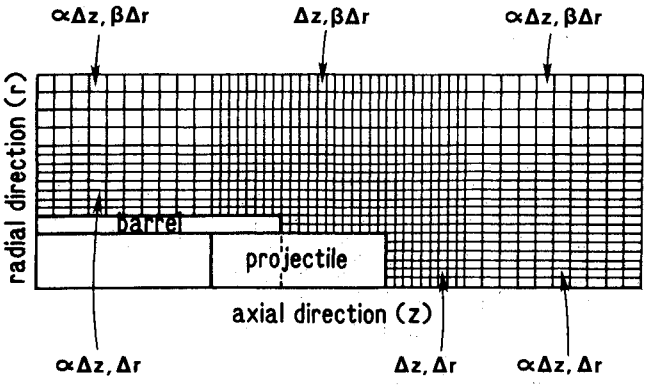

Fig. 1 Sample, fixed but nonuniform, grid mesh: $\alpha > 1.0$; $\beta > 1.0$.

The values of the properties on the centerline can now be determined from the governing equations. A realistic set of ambient conditions is used as the initial conditons. Since the uniqueness of the solution to a set of partial differential equations has not been solved, the well-posedness, which may be interpreted as the success of the boundary conditions and the intial conditions used, can only be determined by the reasonableness of the solution.

Internal Flow

The flow in the barrel, excluding some extreme geometries, is predominantly one-dimensional. Since the emphasis is placed on the muzzle blast flows, the internal flow is computed in a rather approximate fashion; i.e., an isentropic flow of a perfect gas. The propellant is assumed to be burnt completely before it reaches the barrel. This set of assumptions, which is shown in the literature[15] to be adequate, reduces the internal flow to a time-dependent, compressible, one-dimensional, isentropic flow of perfect gases. Therefore, the governing equations are the Euler equations with the corresponding energy and state equations. The normal shock in the barrel is fitted-in and followed in time, with the jump conditions across it being the Rankine-Hugoniot equations. The boundary condition at the projectile base and nose is that the gas-particle velocity is equal to the velocity of the projectile. The properties at the muzzle are computed by the external flow calculations, and transferred in through the communication of the internal/external flows. The barrel inlet conditions are extrapolated from the upstream flow. It is assumed that there is no propellant gas leak between the projectile and the barrel.

Turbulence Modeling

The flowfield generated with the launch of a projectile is highly turbulent due to the existence of a jet flow, a wake flow, and wall turbulent shear flows. Since the simulation of the dynamics of turbulence is still unattainable, a turbulence model is appropriated. A model that would not add to the number of equations of the existing set of governing partial differential equations is an algebraic eddy-viscosity model (zero-equation model). The model of Cebeci,[16] with the improvement of Baldwin and Lomax[17] to do without the need for the thickness of the boundary layer, is used. In this model, the length scales are based on the vorticity distribution rather than the displacement thickness.

Turbulence of the wall shear flow is called the inner turbulence, and it is modeled using the Prandtl mixing-length theory with the improvement of the Van Driest formulation. Using the nomenclature of Baldwin and Lomax,[17] the inner eddy-viscosity coefficient is calculated as

$$(\mu_t)_{\text{inner}} = \rho \ell^2 |\omega| \tag{13}$$

where

$$\ell \cong 0.4y[1 - \exp(-y^+/26)] \tag{14}$$

and

$$y^+ = (\rho_w \tau_w)^{1/2} y/\mu_w \tag{15}$$

where y is the local normal distance from a solid surface.

Turbulence of the outer region is based on the Clauser formulation using the Klebanoff approximation to the Gaussian error function, which gives the intermittency factor. The outer eddy-viscosity coefficient is calculated as

$$(\mu_t)_{\text{outer}} = 0.0269 \rho F_{\text{wake}} F_{\text{Kleb}} \tag{16}$$

where the value of F_{Kleb}, the Klebanoff intermittency factor, is given by

$$F_{\text{Kleb}} = [1 + 5.5(0.3y/Y_{\max})^6]^{-1} \tag{17}$$

and

$$F(y) = y|\omega|[1 - \exp(-y^+/26)] \tag{18}$$

where $F(y)$ is maximum, $F_{\max}$, at $y = Y_{\max}$. F_{wake} is the minimum of $(Y_{\max} F_{\max})$ or $(0.25 Y_{\max} U_{\text{dif}}^2 / F_{\max})$, where

$$U_{\text{dif}} = \{\max |M/\rho| - \min |M/\rho|\} \tag{19}$$

at a fixed tangential location. The crossover point where the switch is made from $(\mu_t)_{\text{outer}}$ to $(\mu_t)_{\text{inner}}$, is the minimum value of y where $(\mu_t)_{\text{outer}}$ becomes less than $(\mu_t)_{\text{inner}}$.

Shock Treatment

A shock-capturing scheme is devised to treat the discontinuities that are rapidly moving and changing their shapes and strengths. It is evident from the continuity equation that, for a compressive wavefront, the divergence of the momentum vector is a negative quantity. Therefore, the detection of shock points is possible through a check of the sign of the momentum vector. To smear these points of discontinuity nonphysically in order to obtain continuous variations of properties, artificial dissipative terms are added to the governing equations. These terms are obtained as follows:

Let the shock thickness be $\delta = C(\Delta s)$, where C is a coefficient and

$$\Delta s = (\Delta r \cdot \Delta z)^{1/2} \tag{20}$$

But the shock thickness is given[18] as

$$\delta \cong \frac{8(2\mu + \lambda)}{(1+\gamma)\bar{\rho}(\Delta V)} \tag{21}$$

where $\bar{\rho}$ is the mean density and (ΔV) the velocity jump across the shock. Using Stoke's rule for λ and assuming that $(\bar{\rho}\Delta V) \cong \delta\rho[\nabla \cdot (M/\rho)]$, solve for the artificial viscosity coefficient μ_a,

$$\mu_a = [(3/32)(1+\gamma)C^2]\rho |\nabla \cdot (M/\rho)| (\Delta r \cdot \Delta z) \tag{22}$$

or, by defining a new constant, $C_\mu = (3/32)(1+\gamma)C^2$,

$$\mu_a = C_\mu \rho |\nabla \cdot (M/\rho)| (\Delta r \cdot \Delta z) \tag{23}$$

$$\lambda_a = -(2/3)\mu_a \tag{24}$$

From the Reynolds analogy,

$$k_a = (Pr)(\gamma R/\gamma - 1)\mu_a \tag{25}$$

Also needed is an artificial right-hand side (RHS_a) with a viscous-like term for the continuity equation, which is written as

$$(RHS)_a = C_\rho (1/\rho) \nabla \cdot (\mu_a \nabla \rho) \tag{26}$$

where C_ρ is a constant. Now, a tuning of the values of the three constants, C, C_ρ, and Pr (the Prandtl number), is performed as a compromise between the crispness of the shocks (but rigorous numerical oscillations in the solution) and the artificial smearedness of the shocks (but stable solution). The artificial thickness of the shock is determined in terms of the representative spatial step size, Δs, by the constant C. Typical values used in this investigation are, $C=0.001$, $Pr=0.9$, and $C_p=0.5$. As it evident from Eqs. (23) and (26), the stronger the compression (i.e., the larger the property gradients), the larger the magnitude of the artificial dissipation terms. However, even for the strongest compressions encountered, the value of the artificial viscosity coefficient does not exceed 85% of the real (molecular plus eddy) viscosity coefficient.

Numerical Solution

The governing equations (1-7) are solved using the explicit, predictor-corrector, finite-difference scheme of MacCormack.[19] The method is second-order accurate in both time and space. In regions of relatively larger property gradients, the Courant-Friedrichs-Lewy (CFL) condition for stability necessitates rather small time steps, causing an increase in the total computer time utilized. In order to save some computer time without resorting to an implicit or hybrid formulation, two measures have been taken: variable time step and fixed but nonuniform grid mesh (Fig. 1). Since the phenomenon being examined here is an accelerating flow, a relatively larger time step size is used initially. Following completion of each step, the new step size is predicted from the CFL condition with a Courant number less than 1, using the maximum property values of that time step and the minimum spatial step sizes. Determining the spatial step sizes is a matter of compromise between the computation time and a better resolution. However, once the spatial step sizes are determined, the time step size is bounded by the CFL condition. The fixed but nonuniform grid mesh is finer around the muzzle plane where the gradients are larger. The spatial step sizes Δz and Δr are enlarged by the greater-than-one factors α and β, respectively, since the gradients are known to be attenuating away from the muzzle plane.

The conservation of axial momentum, for example, is approximated as follows: Using the shorthand notation, where

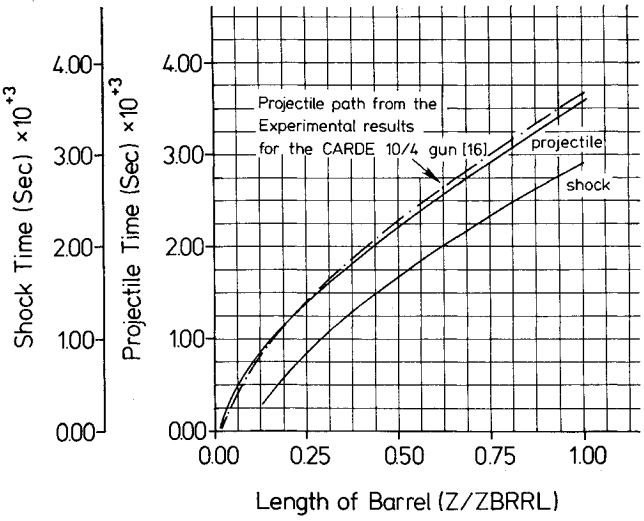

Fig. 2 Time vs travel plots for the projectile and shock inside the barrel.

Δ_z and ∇_z are the forward and backward finite-differencing, respectively, in the axial direction and Δ_r and ∇_r are their counterparts in the radial direction,

Predicted value:

$$\bar{n}^{N+1} = n^N - \Delta t \left\{ \nabla_z \left(p + \frac{n^2}{\rho} \right)^N + \nabla_r \left(\frac{mn}{\rho} \right)^N + \frac{1}{r} \left(\frac{mn}{\rho} \right)^N - \nabla_z \tau_{zz}^N - \nabla_r \tau_{zr}^N - \frac{\tau_{zr}^N}{r} \right\} \tag{27}$$

where

$$\tau_{zz}^N = \frac{4}{3} \mu^N \left[\Delta_z \left(\frac{n}{\rho} \right)^N \right] - \frac{2}{3} \mu^N \left\{ \left[\Delta_r \left(\frac{m}{\rho} \right)^N \right] + \left[\frac{1}{r} \left(\frac{m}{\rho} \right)^N \right] \right\} \tag{28}$$

and

$$\tau_{zr}^N = \mu^N \left\{ \left[\Delta_z \left(\frac{m}{\rho} \right)^N \right] + \left[\Delta_r \left(\frac{n}{\rho} \right)^N \right] \right\} \tag{29}$$

Corrected value:

$$n^{N+1} = \frac{1}{2} (n^N + \bar{n}^{N+1}) - \frac{\Delta t}{2} \left\{ \Delta_z [\overline{p + (n^2/\rho)}]^{N+1} + \Delta_r \left(\frac{\overline{mn}}{\rho} \right)^{N+1} + \frac{1}{r} \left(\frac{\overline{mn}}{\rho} \right)^{N+1} - \Delta_z (\bar{\tau}_{zz})^{N+1} - \Delta_r (\bar{\tau}_{zr})^{N+1} - \frac{1}{r} (\bar{\tau}_{zr})^{N+1} \right\} \tag{30}$$

where

$$\bar{\tau}_{zz}^{N+1} = \frac{4}{3} \bar{\mu}^{N+1} \left[\nabla_z \left(\frac{\bar{n}}{\rho} \right)^{N+1} \right] - \frac{2}{3} \bar{\mu}^{N+1} \left\{ \left[\nabla_r \left(\frac{\bar{m}}{\rho} \right)^{N+1} \right] + \left[\frac{1}{r} \left(\frac{\bar{m}}{\rho} \right)^{N+1} \right] \right\} \tag{31}$$

and

$$\bar{\tau}_{zr}^{N+1} = \bar{\mu}^{N+1} \left\{ \left[\nabla_z \left(\frac{\bar{m}}{\rho} \right)^{N+1} \right] + \left[\nabla_r \left(\frac{\bar{n}}{\rho} \right)^{N+1} \right] \right\} \tag{32}$$

During the course of the computations, some numerical oscillations, attributed largely to the existence of large pressure gradients coupled with the frequent changes in the sign of the momentum, have been experienced. To avoid the possible erroneous drainage of the conserved properties due to these oscillations, the coefficients of the artificial dissipative terms [Eqs. (23-26)] were cautiously increased. The consistency of the solution was checked by refining the grid mesh that enhanced the results. The round-off error was minimized by increasing the number-crunching (double precision) of the computer. The truncation error is of third-order since the scheme is second-order accurate. Since more differenced terms are used in any second-order vs first-order scheme, the discretization error is relatively larger.

Spherical-Symmetry Calculations

The methods of dimensional analysis may be used to solve the problem of one-dimensional unsteady motion of a compressible fluid. The general character of the problems for which self-similarity exists is that the system of dimensional parameters, prescribed partially by the boundary conditions and partially by the initial conditions, must not contain more

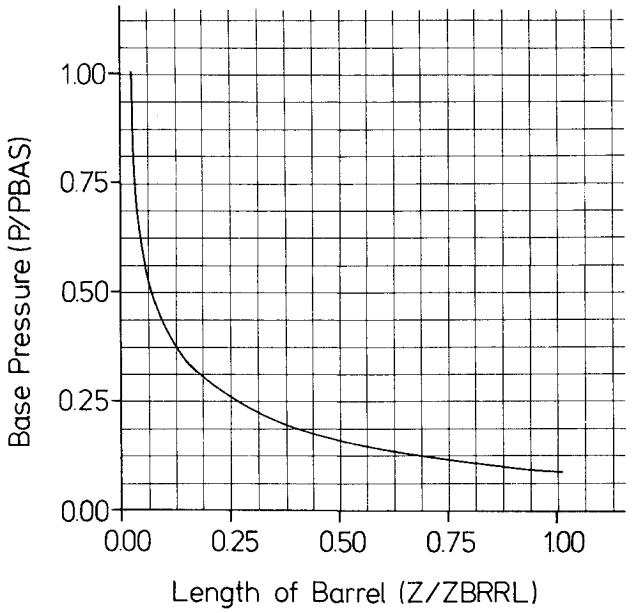

Fig. 3 Pressure at projectile base vs projectile travel inside the barrel; propellant expansion.

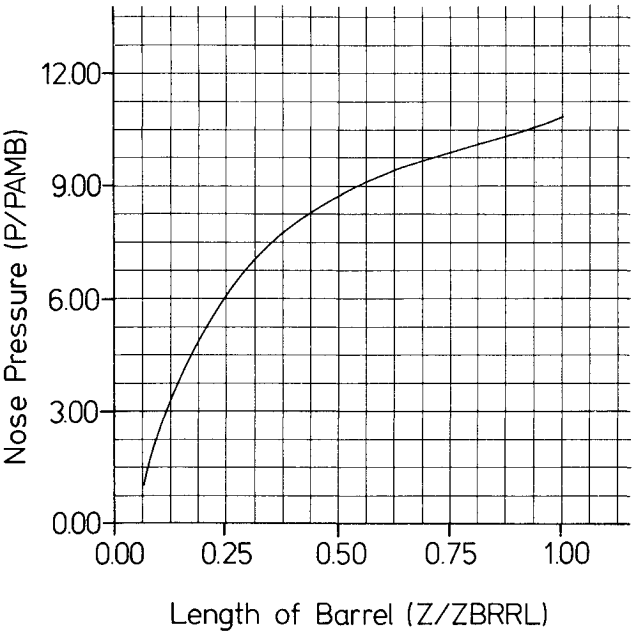

Fig. 4 Pressure at projectile nose vs projectile travel inside the barrel; precursor flow compression.

than two parameters with independent dimensions other than time or length.[3] Therefore, if the blast waves are assumed to be spherically symmetric, and the variation of the back pressure of the waves is neglected, the problem is self-similar, i.e.,

$$\rho,m,p=f(\rho_b,E,r,t) \tag{33}$$

where ρ_b is the back density of the wave. However, the inclusion of the variation of the back pressure, i.e.,

$$\rho,m,p=f(p_b,\rho_b,E,r,t) \tag{34}$$

makes the problem non-self-similar. Sedov[3] gave a closed-form, but numerically attainable, solution to this problem, which is used in the present study to compare its results with the classical blast wave theory. The solution reduces the governing equations of the spherical blast into a set of linear

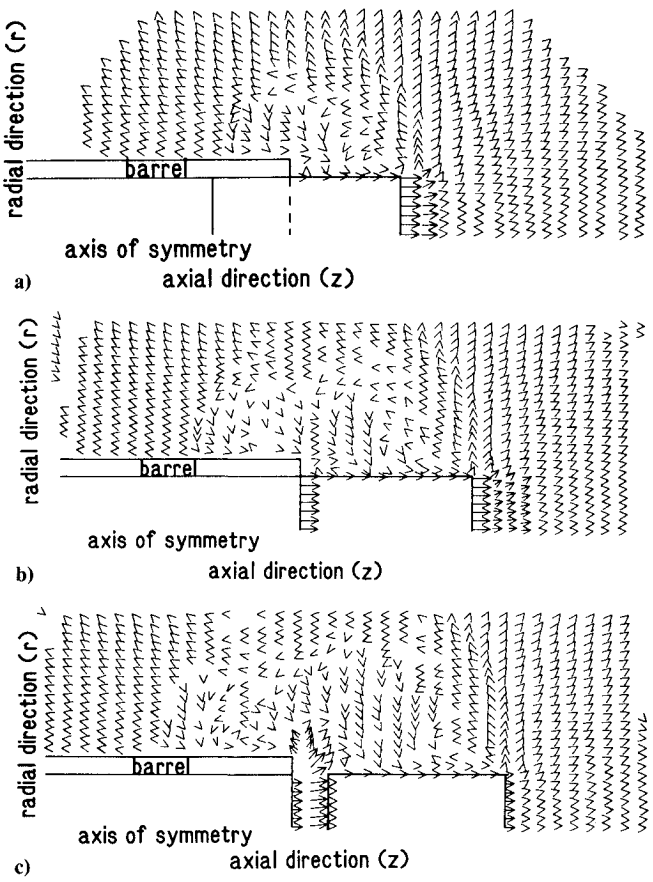

Fig. 5 Growth of flowfield with velocity vectors at 0.05-ms intervals. In frame (c) gas ejection velocity is 340 m/s at the muzzle plane and 240 m/s at the shock front.

differential equations with two independent, nondimensional, self-similarity variables, and one abstract constant which causes the non-self-similarity. Therefore, obtained using this solution technique are: the radius and the property values at the wavefront as functions of the time (propagation), the spatial variation of the properties within the radius of the pressure wavefront at a given time (wave profile), and the temporal variation of the properties at a given location within the radius of the wavefront (attenuation).

Results and Discussion

The numerical model formulated herein simulates the muzzle-blast waves and the related barrel-muzzle flows with the motion of the projectile being followed in time. The output of numerous runs of the computer code enables the analysis of this phenomenon. To establish the integrity of the internal part of the code, which is the source of the muzzle-plane data, a time-travel plot of the projectile and the internal shock is included (Fig. 2). The experimental results for the CARDE 10/4 gun[20] are normalized and superimposed. The fast decay of the pressure at the base of the projectile (Fig. 3) and the compression of gases at the projectile nose (Fig. 4) are also computed and plotted. Despite the limiting assumptions made for the barrel flow computation regarding the combustion and nature of the propellant gases, the solution is highly accurate and reliable. This should also be partially attributed to the data provided by the external flow computation when it is turned on after the ejection of the shock.

The pressure-induced, projectile-driven muzzle flow is depicted with the aid of velocity vectors (Fig. 5). The rapid propagation and strong decay of the pressure waves, including the precursor and blast shocks, are presented in the

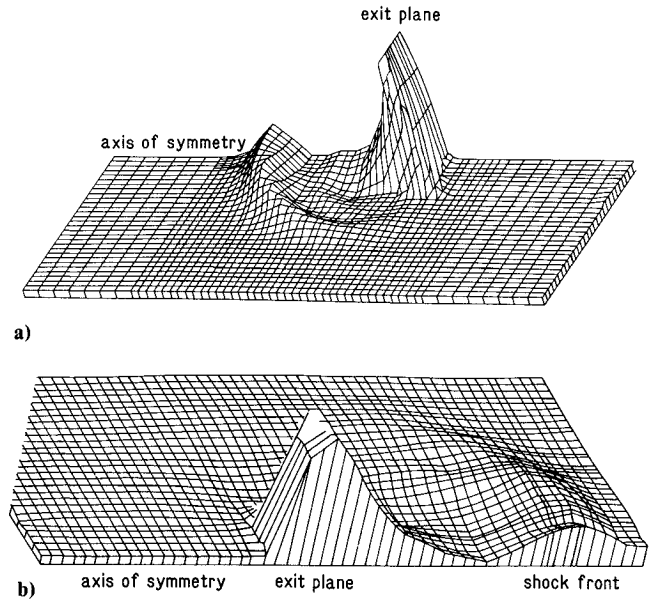

Fig. 6 Pressure waves in a block diagram of pressure vs the computation zone at a) 0.10 and b) 0.15 ms, after the precursor shock clears the muzzle plane.

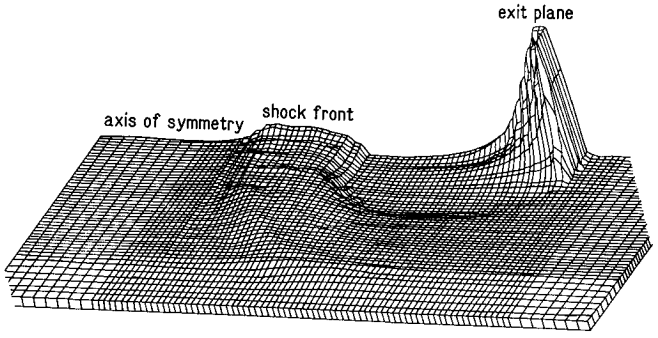

Fig. 7 Postejection pressure waves in a block diagram of pressure vs computation zone 0.3 ms after the blast shock clears the muzzle plane.

form of block diagrams and pressure contours (Figs. 6-8). The case is run with a sample data set. The barrel diameter D is 0.06 m, and the projectile length and weight are 0.10 m and 0.50 kg, respectively.

The shock profiles computed using the spherical-symmetry assumption[3] are overlaid (Figs. 8 and 9) to display the comparison with the axisymmetric computation. In the near field, however, both solutions are believed to be well approximated by the typical power-law variation in time of the classical blast wave theory[4] and the later predictions.[21]

The pressure waves consist of pulses distinguished by the presence of the precursor and the blast shocks. Secondary compressive waves strengthen the main shock waves, but rarefactive waves originating at the corner appear to propagate, weakening this effect. The pressure distribution within the rapidly expanding gases is not uniform, and different in behavior than the free-jet expansion. The underexpanded propellant flow forms a jet with reflections of the pressure waves from the interface with the ambient air. The waveforms change shape in the course of the propagation in quite a different way from that in the small-amplitude case. This is due to the nonlinearity of the phenomenon that causes the flow properties to be largely disturbed. The propagation of the waves seems to be faster in the axial direction, and their decay is more gradual. Therefore, it is believed that the axisymmetric propagation of these waves is deviant

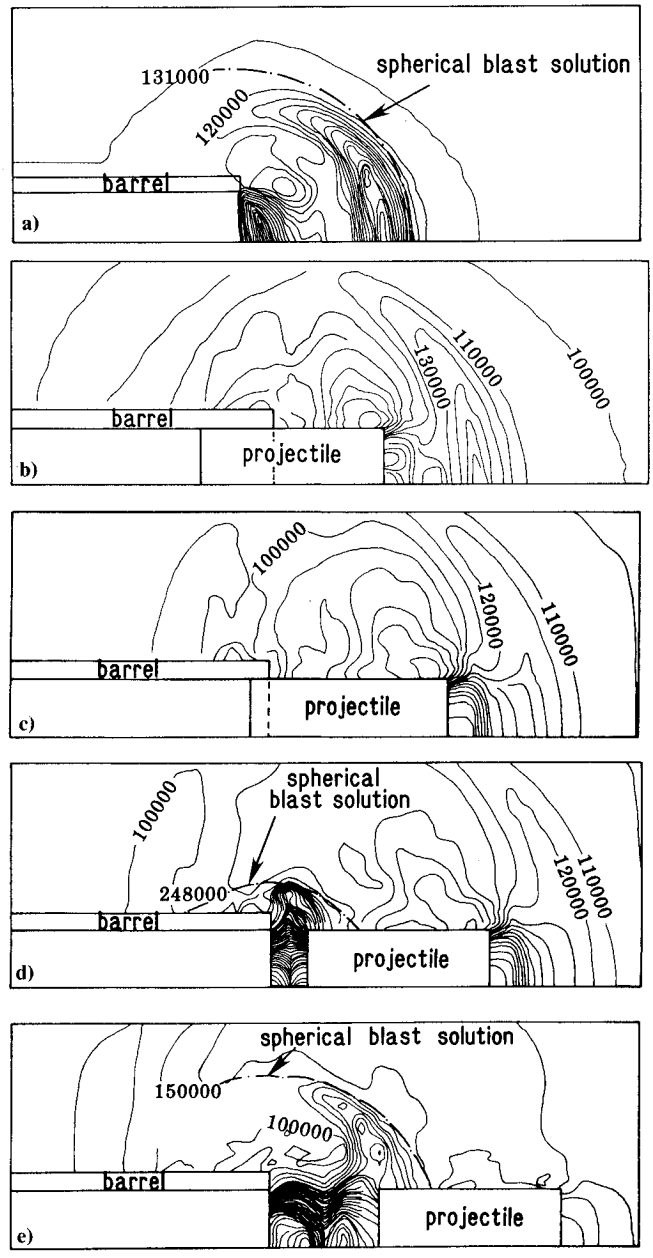

Fig. 8 a) Pressure contours at 0.1 ms after the precursor shock clears the muzzle plane. Prelaunch contours with a contour interval of 2×10^4 N/m^2. b-e) Pressure contours at 0.1-ms intervals during launch.

from the spherical propagation. Low-pressure areas exist in patches following the high-pressure pulses.

It is conclusive that, for all practical purposes, viscosity is relatively small, but its effects essentially control the basic properties. Its effects are dissipative and dispersive; not only the attenuation, but also the propagation patterns are altered due to viscosity. Although its effects are strongest at the regions close to the solid boundaries, they are not confined to those regions. The viscous forces acting near body surfaces reduce the momentum in the boundary-layer regions so that, when acted upon by the initial forces, the boundary layer may separate from the body. This possible separation generates the vortical and unstable shear layers. The unsteadiness is generated not only by the nature of the flow, but also by the pressure field and the viscosity itself. This is an important cause of the changes in the propagation pattern of the pressure waves. Therefore, for a more realistic mathematical model of the muzzle blast, the inclusion of the viscous terms is perceived to be essential.

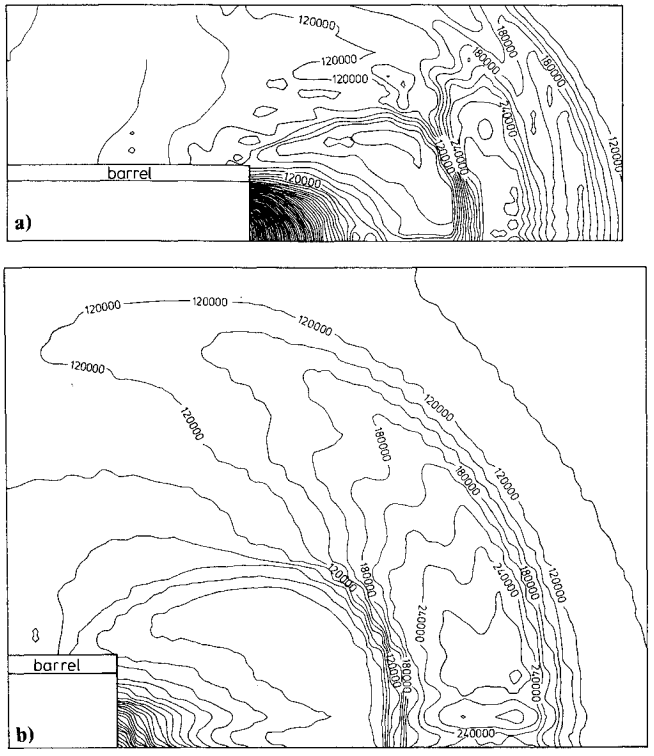

Fig. 9 Pressure contours at a) 0.5 and b) 1.0 ms, after the base of the projectile clears the muzzle plane. Postlaunch contours with a contour interval of 2×10^4 N/m^2.

The large pressure gradients, coupled with the frequent changes in the sign of the velocity and possible separation, may have caused erroneous drainage of the conserved properties. The density undershoots experienced during the calculations seemed to be due to this fact. Increasing the effect of artificial dissipative terms, on the expense of smearing the pressure wavefronts, solved the problem.

Conclusion

Existing analyses of the blast waves had, thus far, excluded the effects of viscosity and the combined study of the internal/external flows of gun barrels. A Navier-Stokes study of these waves has been conducted with the external parameters being related to the internal barrel parameters. MacCormack's explicit finite-difference method has been used to solve the set of governing equations. The results of the study help the analysis of these high-amplitude pressure waves. It is also concluded that the prediction of the spherical-symmetry analysis of classical theory are prohibitively restrictive.

Acknowledgment

The initiation of this study was inspired by Dr. Robert W. Courter, Associate Professor of Mechanical Engineering at Louisiana State University.

References

[1]Schmidt, E. M. and Shear, D. D., "Optical Measurements of Muzzle Blast," *AIAA Journal*, Vol. 13, Aug. 1975, pp. 1086-1091.

[2]Klingenberg, G., Mach, H., and Smeets, G., "Probing of the Unsteady Reacting Muzzle Exhaust Flow of 20-mm Gun," ASME Paper 82-HT-34, 1982.

[3]Sedov, L. I., *Similarity and Dimensional Methods in Mechanics*, Academic Press, New York, 1959, pp. 238-250.

[4]Sakurai, A., "Blast Wave Theory," *Basic Development in Fluid Dynamics*, edited by M. Holt, Academic Press, New York, 1965, pp. 309-375.

[5]Oswatitsch, K., "Intermediate Ballistics," DVL Rept. 358, FB64-27, Deutscheluft und Raumfahrt, W. Germany, 1964.

[6]Traci, R. M., Farr, J. L., and Liu, C. Y., "A Numerical Method for the Simulation of Muzzle Gas Flows with Fluid and Moving Boundaries," SAI Rept. 74-513-LA, Science Applications Inc., El Segundo, CA, 1974.

[7]Romine, G. and Edquist, C. T., "Muzzle Blast from Canister Launched Missile," AIAA Paper 80-1187, 1980.

[8]Erdos, J. I. and Del Guidice, P. D., "Calculation of Muzzle Blast Flowfields," *AIAA Journal*, Vol. 13, Aug. 1974, pp. 1048-1055.

[9]Taylor, T. D. and Lin, T. C., "Numerical Model for Muzzle Blast Flowfields," *AIAA Journal*, Vol. 19, March 1981, pp. 346-349.

[10]Moretti, G., "Muzzle Blast Flow and Related Problems," AIAA Paper 78-1190, 1978.

[11]Zoltani, C., "Computer Simulation of Intermediate Ballistic Environment of a Small Arm, M-16," U.S. Army Ballistic Research Laboratory, Rept. ARD 76-1, 1976.

[12]Baysal, O., "Computational Simulation of Muzzle Blast and the Analysis of Its Propagation," *Proceedings of the Eighth International Symposium on Ballistics*, Orlando, FL, 1984, pp. LD1-LD10.

[13]Baysal, O., "Analysis of High Pressure Waves in Compressible, High-Reynolds-Number Flows Including Viscous Effects," *Multidimensional Fluid Transients*, FED—Vol. 18, ASME Special Publications, New York, 1984, pp. 23-29.

[14]Courant, R. and Freidrichs, K. D., *Supersonic Flow and Shock Waves*, Interscience Publishers, New York, 1948.

[15]Seigel, A. E., *The Theory of High Speed Guns*, AGARDograph 91, 1965.

[16]Cebeci, T., "Calculation of Compression Turbulent Boundary Layers with Heat and Mass Transfer," AIAA Paper 70-741, 1970.

[17]Baldwin, B. S. and Lomax, H., "Thin Layer Approximation and Algebraic Model for Separated Turbulent Flows," AIAA Paper 78-257, 1978.

[18]Thompson, P. A., *Compressible Fluid Dynamics*, McGraw-Hill Book Co., New York, 1972, pp. 517-525.

[19]MacCormack, R. W. and Lomax, H., "Numerical Solution of Compressible Viscous Flows," *Annual Review of Fluid Mechanics*, Vol. 11, 1979, pp. 289-316.

[20]Murphy, J. R. B., Badhwar, L. K., and Lavoie, G. A., "Interior Ballistic Calculation Systems for Light Gas Guns and Conventional Guns," Computing Devices of Canada, Ottawa, Rept. 70-12, 1970.

[21]Freeman, R. A., "Variable-Energy Blast Wave," *British Journal of Applied Physics*, Ser. 2, Vol. 1, 1968, pp. 214-219.